[Fe(abpt)$_2$(NCSe)$_2$] polymorph A: Structural studies into the spin crossover behaviour

Helen E. Mason,[a] Michelle L. Hamilton,[b] Judith A. K. Howard[a] and Hazel A. Sparkes[c]*

Received 00th January 20xx,
Accepted 00th January 20xx

DOI: 10.1039/x0xx00000x

www.rsc.org/

The spin crossover behaviour of [Fe(abpt)$_2$(NCSe)$_2$] (abpt = 4-amino-3,5-bis(pyridin-2-yl)-1,2,4-triazole) polymorph **A** has been examined using single crystal X-ray diffraction and variable temperature UV-Vis transmission spectroscopy. The crystal structure of **A** is reported at sixteen temperatures between 30 and 375 K, all of which are in the monoclinic space group $P2_1/n$ with Z' = 0.5. Changes in the crystallographic cell parameters, bond lengths, distortion parameters and intra and intermolecular interactions between 375 K and 30 K are discussed. Continuous irradiation with a 670 nm, 5 mW CW laser at 30 K enabled a light induced excited spin state trapping (LIESST) metastable high spin structure, HS*, to be obtained.

Introduction

Spin crossover in molecular compounds was first observed in the 1930s.[1] Despite having been extensively studied it still attracts significant research interest partly due to its potential for industrial applications,[2-4] for example in data storage devices,[5, 6] molecular magnets[7] and molecular switches.[8, 9] For a spin crossover compound changes in the physical environment,[10] including temperature,[11] pressure,[12, 13] magnetic field or light irradiation,[14, 15] can result in a reversible change in the spin state. Many of the spin crossover complexes that have been identified and studied are octahedral Fe(II) species[10, 16] but spin crossover is also relatively common for other octahedral 3d^4-3d^7 metal centres such as Fe(III)[15, 17] or Co(II).[18, 19] In the solid state, spin crossover is a complex phenomenon and the abrupt or gradual nature, completeness and temperature at which it occurs have been linked to the presence of intermolecular interactions within the crystal lattice. Indeed different polymorphs of the same compound can show different spin crossover behaviour.[20-23] Spin crossover complexes with limited cooperative communication between metal centres display very gradual changes in spin state, while species with significant molecular cooperativity show abrupt changes in spin state often with hysteresis. In addition, spin crossovers can be complete, partial or stepped.[24, 25] Insights into spin crossover materials and their behaviour are coming from a range of techniques including magnetic data,[13, 26] X-ray crystallography,[11, 27] spectroscopic techniques including UV-Vis,[26, 28] Resonant Ultrasound,[29] Mossbauer[11, 30] and X-ray photoelectron spectroscopy.[27] Given the complexity of spin crossover behaviour,[26, 31] it is important to study such systems in detail to further our understanding and allow the customised design of spin crossover materials for desired applications.

Spin crossover behaviour has been identified in various Fe(II) complexes containing 3,5-bis(pyridin-2-yl)-1,2,4-triazole derivatives with *trans* NCS or NCSe ligands: for example, *trans*-[Fe(MBPT)$_2$(NCS)$_2$][32] (MBPT = 4-*p*-methylphenyl-3,5-bis(pyridine-2-yl)-1,2,4-triazole), $T_{1/2}$ ~ 231 K; [Fe(L^{pz})$_2$(NCS)$_2$][33] (L^{pz} = 4-*p*-tolyl-3-(2-pyrazinyl)-5-(2-pyridyl)1,2,4-triazole) which exhibits an incomplete change in spin state $T_{1/2}$ (cooling) = 142 K, $T_{1/2}$ (warming) = 149 K; and [Fe(L^{pz})$_2$(NCSe)$_2$],[33] $T_{1/2}$ (cooling) = 172 K, $T_{1/2}$ (warming) = 177 K. [Fe(pldpt)$_2$(NCS)$_2$][34] (pldpt = *N*^{4}-pyrrol-3,5-di(2-pyridyl)-1,2,4-triazole), which has both *cis* and *trans* coordinated (2:1 ratio) NCS ligands around the Fe centre, displays interesting spin crossover behaviour. Only the Fe centres which have *trans* coordinate NCS ligands (i.e. one-third of the Fe centres) display a thermal spin crossover, with $T_{1/2}$ being affected by the presence of solvent (solvent free $T_{1/2}$ = 180 K, solvated $T_{1/2}$ < 89 K). In addition, four polymorphs of [Fe(abpt)$_2$(NCS)$_2$] (abpt = 4-amino-3,5-bis(pyridin-2-yl)-1,2,4-triazole) (**2**) have been identified (Table 1); three of which, polymorphs **A**,[29, 35, 36] **C**[37] and **D**[38] (herein referred to as **2A**, **2C** and **2D**), display thermal spin crossover. **2A** exhibits a gradual thermal spin crossover without hysteresis and with $T_{1/2}$ = 180 K[36] (re-measured as $T_{1/2}$ = 188 K for crystals prepared using a different method).[39] **2C** and **2D** have two crystallographically unique Fe centres and display more complicated spin crossover behaviour. In **2C**, one of the Fe centres undergoes a thermal spin crossover with $T_{1/2}$ = 86 K. Both temperature and light induced excited spin state trapping (TIESST and LIESST) have been observed and result in a commensurate modulated structure with four crystallographically independent Fe centres.[37] In the case of **2D**, thermal spin crossover of one of the crystallographically independent Fe centres has been reported with $T_{1/2}$ = 162 K. At low temperature, as well as the occurrence of LIESST, photoinduced linkage isomerism of the NCS ligand is observed.[38] The final polymorph, **B**[40] (herein referred to as **2B**), undergoes a thermal spin crossover at pressures >4.4 kbar but not at ambient pressure.[40]

Two polymorphs of the title compound, [Fe(abpt)$_2$(NCSe)$_2$] **A**[36] and **B**,[40] have been reported previously (Table 1). While polymorph **B** does not undergo thermal spin crossover between 2 - 300 K,[40] polymorph **A** has been shown to undergo a thermal spin crossover without hysteresis and with $T_{1/2}$ = 224 K.[36] Magnetic studies on precipitated microcrystalline or single crystal samples of **A** have shown either a residual HS fraction, γ_{HS}, of 14%[35] or a virtually complete spin crossover[36] respectively. Both polymorphs have a six-coordinate Fe(II) centre with the NCSe ligands *trans* to each other. The structures of [Fe(abpt)$_2$(NCSe)$_2$] polymorphs **A** and **B** are isostructural to those of the sulphur analogue, **2A**[36] and **2B**.[40] The 293 K HS

[a] *Department of Chemistry, Durham University, South Road, Durham, DH1 3LE, UK.*
[b] *RAL Space, STFC, Rutherford Appleton Laboratory, Didcot, OX11 0QX, UK.*
[c] *Department of Chemistry, University of Bristol, Cantock's Close, Bristol, BS8 1TS, UK. E-mail: hazel.sparkes@bristol.ac.uk.*

Electronic Supplementary Information (ESI) available: Additional crystal data not in the main paper, summary of hydrogen bonding parameters and π-π contacts as a function of temperature, CCDC 1856782-1856790 and 1862057-1862064. See DOI: 10.1039/x0xx00000x

Table 1 - Brief summary of the spin crossover behaviour of $[Fe(abpt)_2(NCSe)_2]$ and $[Fe(abpt)_2(NCS)_2]$ (2) polymorphs.

Complex	Polymorph colour and habit	Reference number herein	Spin crossover behaviour
$[Fe(abpt)_2(NCSe)_2]$	**A** red block	**A**	Gradual complete thermal spin crossover without hysteresis, $T_{1/2}$ = 224 K, residual Y_{HS} = ~0% at low temperature. LIESST observed with T_{LIESST} = 32 K.[36]
	B orange prism	**B**	Thermal spin crossover not observed at ambient pressure.[40]
$[Fe(abpt)_2(NCS)_2]$	**A** dark red block	**2A**	Gradual thermal spin crossover without hysteresis, $T_{1/2}$ = 180 K[36] (188 K),[39] residual Y_{HS} = 23% (~0%)[39] at low temperature. LIESST observed with T_{LIESST} = 40 K.
	B orange prism	**2B**	Incomplete thermal spin crossover at >4.4 kbar, $T_{1/2}$ = 65 K, becoming more complete with increased pressure.[40]
	C red block	**2C**	Thermal spin crossover of one Fe centre in the asymmetric unit, $T_{1/2}$ = 86 K. Commensurate modulated structure with the *c*-axis length tripled observed in TIESST and LIESST metastable states and between 170 - 86 K upon slow cooling.[37, 39]
	D red needle	**2D**	Thermal spin crossover of one Fe centre in the asymmetric unit, $T_{1/2}$ = 162 K. Two low temperature light induced metastable processes: LIESST, T_{LIESST} = 36 K, and photoinduced NCS to SCN linkage isomerism.[38, 39]

structure of **A** is known, however LS and LIESST HS* structures have not been previously characterised and are reported herein alongside a detailed crystallographic study of structural changes occurring during the spin crossover. Single crystal variable temperature UV-Vis transmission spectroscopy, which has been used to monitor spectral changes across the thermal spin crossover temperature range, supports the crystallographic evidence and helps to provide further insight into the spin crossover behaviour of **A**.

Experimental

Synthetic procedures

X-ray diffraction quality single crystals of $[Fe(abpt)_2(NCSe)_2]$ polymorph A were produced using the slow diffusion method previously reported for the synthesis of $[Fe(abpt)_2(NCS)_2]$.[39] All precursor materials are commercially available and were used as received, solvents were degassed and manipulations carried out under a nitrogen atmosphere. $FeSO_4.7H_2O$ (0.5 mmol, 0.139 g) and KNCSe (1 mmol, 0.144g) were stirred in MeOH (8 ml) for 15 min, the resulting pale yellow K_2SO_4 precipitate removed by filtration and deionised H_2O (8 ml) added to the remaining clear solution. abpt [4-amino-3,5-bis(pyridin-2-yl)-1,2,4-triazole] (1 mmol, 0.238 g) dissolved in MeOH (10 ml) was transferred to a narrow (<5 cm) Schlenk tube and the $Fe^{2+}/2(NCSe)^-$ solution carefully injected into the bottom of the Schlenk to form a layer underneath the abpt solution. A red coloured band immediately formed at the interface between the two layers. Single crystals of polymorph **A** suitable for X-ray diffraction studies were formed within 1-4 weeks but no crystals of polymorph **B** were produced.[40]

X-ray Crystallography - Variable temperature and LIESST measurements

A Bruker Smart 1K CCD diffractometer was used to collect single crystal X-ray diffraction data using graphite monochromised

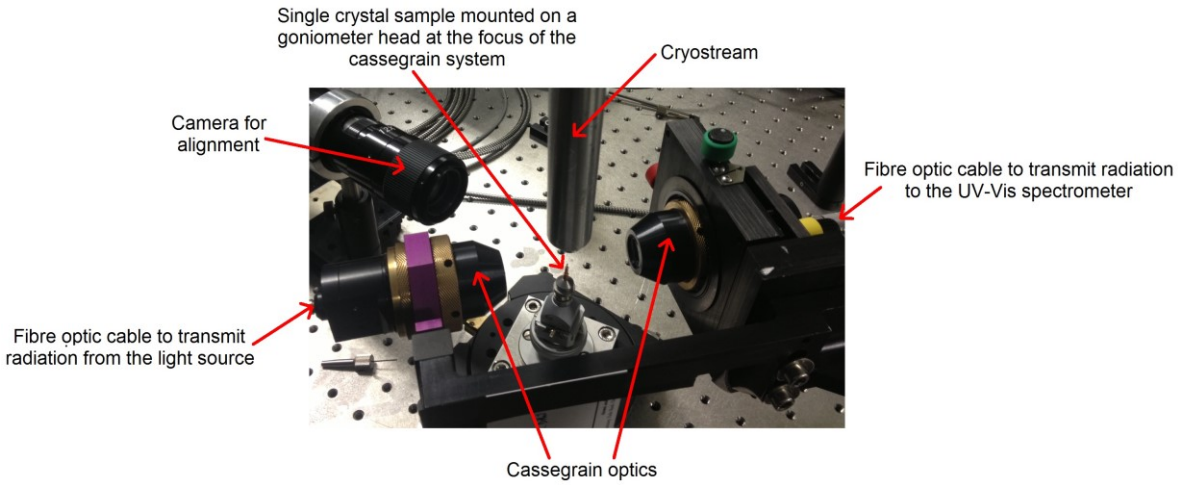

Figure 1 - Annotated photograph showing the custom built system used to collect variable temperature single crystal UV-Vis transmission spectra.

Mo*Kα* (λ = 0.71073 Å) X-ray radiation. Cooling was achieved using either an Oxford Instruments open flow nitrogen Cryostream or an Oxford Cryosystems HeliX[41] for datasets collected at temperatures >105 K or <105 K respectively. Data collection was carried out using SMART software,[42] integration performed using SAINT[43, 44] and face indexed numerical absorption corrections applied using SADABS-2012/1.[45] The structures were solved by direct methods in SHELXS[46] and refined by full matrix least squares on F^2 in SHELXL[46] in Olex2.[47] Non-hydrogen atoms were refined anisotropically and all hydrogen atoms were located geometrically and refined using a riding model except for the N6 hydrogen atoms which were located in the difference map. A LIESST HS* structure was obtained at 30 K by irradiating a crystal *in-situ* using a 670 nm, 5 mW CW laser. To establish and maintain a photostationary state (i.e. the metastable LIESST HS* structure) for the duration of the data collection, the crystal was irradiated for 60 min prior to and also throughout the data collection. Due to deterioration of the crystal quality during heating-cooling cycles and upon irradiation, different crystals were used for data collections with the HeliX (Crystal **1**; full datasets at 30, 50, 75, 100 and 30 K under laser irradiation) and Cryostream (Crystal **2**; full datasets at 108, 125, 150, 175, 225, 275, 325 and 375 K). Full structure determinations were carried out at sixteen temperatures these structures and the structure at 30 K under irradiation are published herein, see Table 2 and ESI Table S1.

Relaxation of the LIESST HS* state was examined by monitoring the evolution of unit cell parameters with time. Immediately after switching off the laser, omega scans consisting of 30 frames (scan width 0.4°) at alternating phi positions of 0 and 90° were collected continuously until the crystal had relaxed back to the LS state. SMARTreduce,[48] a script which automates reflection harvesting, unit cell indexation and least squares refinement in SMART,[42] was used to iteratively determine a unit cell from each consecutive set of two runs.

Variable temperature UV-Vis transmission spectroscopy

Variable temperature single crystal UV-Vis transmission spectroscopy was carried out using a custom built setup[29] (Figure 1) based on a cassegrain system (Bruker). Radiation from a Hamamatsu high power UV-VIS fiber broadband light source (L10290) was transferred via fibre optic cables to the cassegrain optics and into an Andor Shamrock SR-303i imaging spectrograph coupled with a Newton EMCCD camera (150 lines/mm grating groove density; specifications quote a resolution of 0.88 nm at a centre wavelength of 500 nm). The spot size at the focus of the cassegrain optics is determined by the input fibre optic cable core size; this was chosen such that a

Table 2 - Crystal data and refinement results for **A** at 375 K, 30 K and 30 K after irradiation.

Spin state (temperature)	**HS [375(2) K]**	**LS [30(2) K]**	**LIESST HS* [30(2) K]**
Empirical formula	$C_{26}H_{20}FeN_{14}Se_2$	$C_{26}H_{20}FeN_{14}Se_2$	$C_{26}H_{20}FeN_{14}Se_2$
Formula weight	742.33	742.33	742.33
Temperature / K	375(2)	30(2)	30(2)
Crystal system	monoclinic	monoclinic	monoclinic
Space group	$P2_1/n$	$P2_1/n$	$P2_1/n$
a / Å	8.6568(4)	8.4320(6)	8.5189(7)
b / Å	10.2722(5)	9.9499(7)	10.0940(8)
c / Å	16.6275(8)	16.3484(12)	16.4616(13)
β / °	93.5349(9)	93.1202(14)	93.1989(15)
Volume / Å^3	1475.78(12)	1369.6(2)	1413.3(2)
Z	2	2	2
ρcalc / (g/cm^3)	1.671	1.800	1.744
μ / mm-1	3.022	3.256	3.155
F(000)	736.0	736.0	736.0
Radiation	MoKα (λ = 0.71073 Å)	MoKα (λ = 0.71073 Å)	MoKα (λ = 0.71073 Å)
2θ range for data collection / °	4.664 to 52.738	4.794 to 56.554	4.736 to 55.756
Index ranges	-10 ≤ h ≤ 10, -12 ≤ k ≤ 12, -19 ≤ l ≤ 20	-11 ≤ h ≤ 11, -12 ≤ k ≤ 13, -21 ≤ l ≤ 19	-11 ≤ h ≤ 11, -13 ≤ k ≤ 13, -20 ≤ l ≤ 21
Reflections collected	14338	9605	11585
R_{int}	0.0396	0.0353	0.0428
Data/restraints/parameters	3018/0/202	3381/0/202	3362/0/202
Goodness-of-fit on F^2	1.076	1.035	1.092
Final R indexes [I>=2σ (I)]	R_1 = 0.0410, wR_2 = 0.0953	R_1 = 0.0362, wR_2 = 0.0726	R_1 = 0.0452, wR_2 = 0.0922
Final R indexes [all data]	R_1 = 0.0716, wR_2 = 0.1094	R_1 = 0.0459, wR_2 = 0.0754	R_1 = 0.0523, wR_2 = 0.0949
Largest diff. peak/hole / (e Å-3)	0.85/-0.70	0.90/-0.74	2.14/-1.21

~50 µm diameter region of the crystal was sampled by UV-Vis radiation.

A single crystal fragment (<100×100×25 µm), mounted using perfluoropolyether oil onto a 100 µm aperture UV-Vis MicroLoop (MiTeGen, LLC) fixed on an XRD goniometer head, was positioned at the focus of the cassegrain system in the orientation giving the cleanest spectroscopic signal. The crystal was observed using a high-magnification zoom lens system mounted on a Thorlabs CMOS camera. An Oxford Cryosystems non-liquid nitrogen Cobra Cryostream was used to control the sample temperature.

To monitor spectral changes with temperature, Andor's Solis software was used to collect spectra in kinetic series mode (100 ms exposure, 30 s kinetic cycle time) while cooling from 290 K to 83 K at 150 K/hr. Spectra were presented by the Solis software in absorbance mode by collecting background (no light source) and reference (light source on a MicroLoop without sample) spectra. All data were normalised for comparison because the % transmission, but not the spectral shape, is dependent on the crystal orientation within the light beam. A Savitzky-Golay smoothing filter (polynomial order 2, frame size 13) was applied to the normalised data using MATLAB.[49] MATLAB[49] functions "polyfit" and "polyval" were used to give an estimate of the standard error in the Savitzky-Golay fitted value at a chosen wavelength of interest.

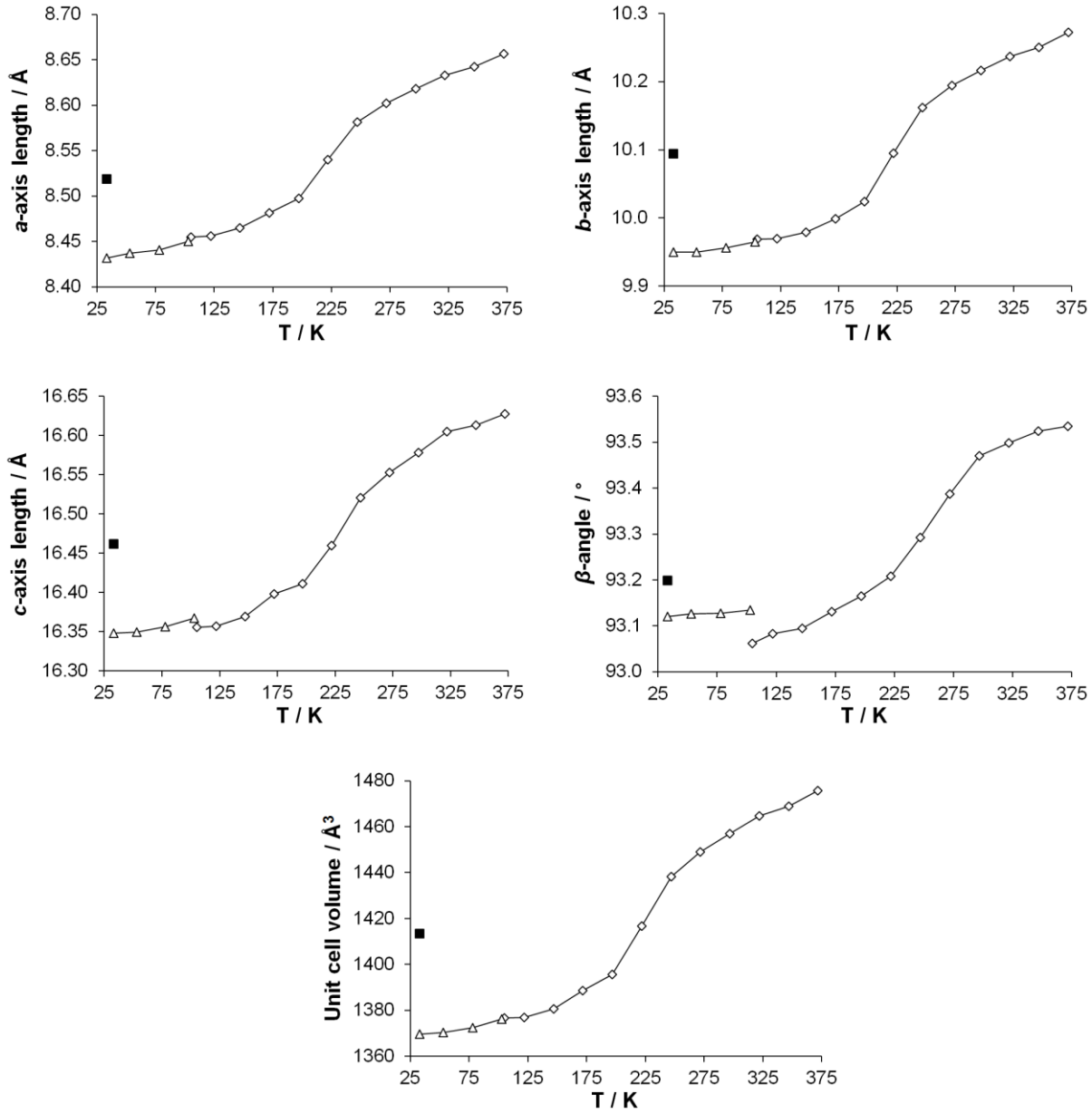

Figure 2 -Cell parameters for **A** measured as a function of temperature: (◊) and (Δ) data collected using the Cryostream (Crystal 2) and HeliX (Crystal 1) respectively; (■) cell parameters for the LIESST HS* state (Crystal 1). Error bars are included but obscured by the data point markers.

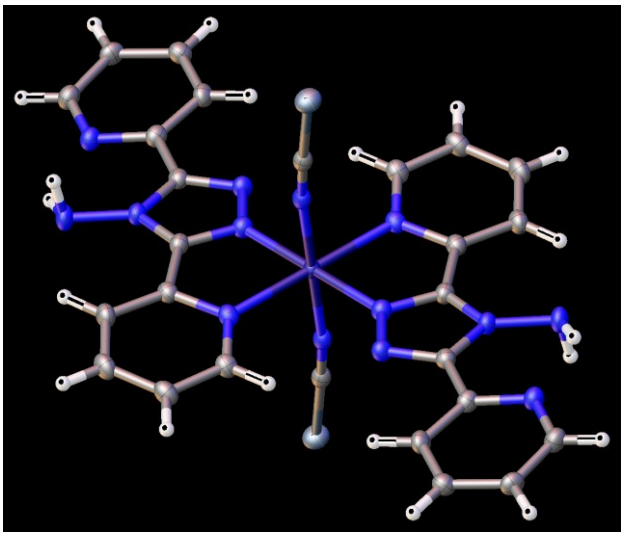

Figure 3 - Crystal structure of $[Fe(abpt)_2(NCSe)_2]$ polymorph **A** at 125 K with ellipsoids depicted at 50% probability level. The asu consists of half a molecule and 'i' represents the other half of the molecule which is related by the symmetry operator 1-*x*, 1-*y*, 1-*z*.

Results and discussion

Thermal spin crossover and cell parameter changes

The reported magnetic data for $[Fe(abpt)_2(NCSe)_2]$ polymorph **A** shows a gradual thermal spin crossover without hysteresis between ~265 – 175 K with $T_{1/2}$ = 224 K[36]. The occurrence of this spin crossover was also clearly indicated, over the expected region, through changes in the crystallographic cell parameters of **A** upon cooling from 375 to 30 K, with an ~0.3 Å decrease in the length of all of the cell axes and an ~0.4° decrease in the *β*-angle (Figure 2, Table 2 and ESI Table S1). This resulted in an ~8% decrease in the unit cell volume over the full temperature range investigated.

The HS structure of **A** described in this paper is consistent with the previously reported structure of **A** at 293 K[36, 40], since all of the structures determined herein have significant similarities the 125 K structure is used for the following discussion of the key structural features (Figure 3). **A** crystallises in the monoclinic space group $P2_1/n$ with half a molecule in the asymmetric unit (Z' = 0.5, Z = 2); the full molecule consists of a 6-coordinate iron metal centre bound to two abpt (each coordinated through both a pyridyl and a tiazole nitrogen) and two NCSe ligands. The two NCSe ligands are coordinated *trans* to each other and are approximately linear with an N1-C1-Se1 bond angle of 177.8(2)°, however the NCSe is slightly bent with respect to the iron metal centre with an Fe1-N1-C1 bond angle of 171.4(2)°. The N-Fe-N angles between the NCSe and abpt ligands range from 87.96(8) - 92.03(8)°. The abpt ligands are slightly distorted from planarity; there is an angle of 10.8(1)° between planes calculated through the two 6-membered pyridyl rings and angles of 9.0(1)° and 11.4(1)° between the 5-membered triazole ring and either of the pyridyl (N7, C9-C13) or (N2, C2-C6) rings respectively. An intramolecular hydrogen bond is present between N6-H6B···N7 for which D-H = 0.94(3) Å, H···A = 2.09(3) Å, D···A = 2.853(3) Å, <DHA = 138(2)º, along with a weak intramolecular C2-H2···N4#1 (#1 = 1-*x*, 1-*y*, 1-*z*) interaction with D-H = 0.95 Å, H···A = 2.35 Å, D···A = 3.132(3) Å, <DHA = 140º. In addition, a short intermolecular N6-H6A···Se1#2 (#2 = 1/2+*x*, 3/2-*y*, 1/2+*z*) interaction for which D-H = 0.96(3) Å, H···A = 2.65(3) Å, D···A = 3.476(2) Å, <DHA = 145(2)º was identified. The structure also contains π-π contacts with a centroid (N2, C2-C6) to centroid (N7#3, C9#3-C13#3, #3 = 1-*x*, 2-*y*, 1-*z*) distance of 3.684(1) Å and an offset of 1.432(4) Å. These π-π contacts create a 1-dimensional chain through the lattice in the approximate direction of the *b*-axis (Figure 4).

The structure determined at temperatures between 375 - 30 K (ESI Table S1,S3-S5) show that, although the key structural

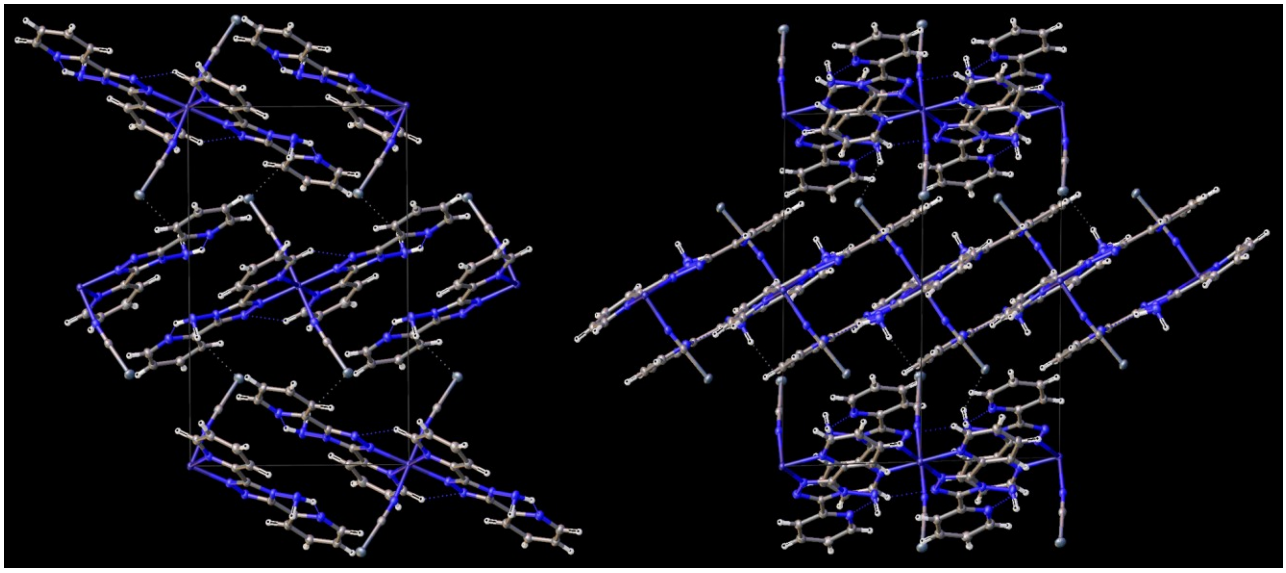

Figure 4 - Diagrams showing the packing of $[Fe(abpt)_2(NCSe)_2]$ polymorph **A** at 30 K viewed along the (left) (100) and (right) (110) directions.

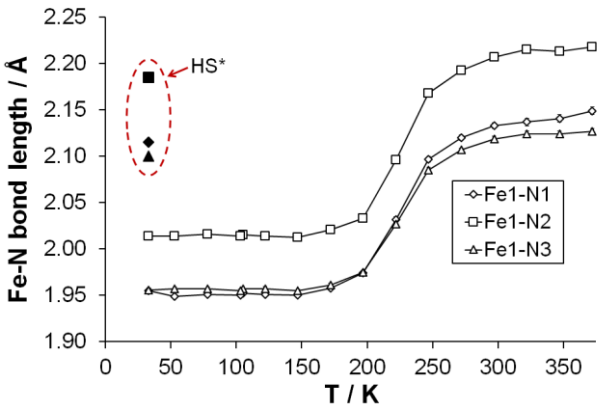

Figure 5 - Change in Fe-N bond lengths as a function of temperature, LIESST HS* values are contained within the dashed oval. Error bars are included but obscured by the data point markers.

features of **A** discussed above are not significantly altered as a result of the spin crossover, there are changes in some of the geometric parameters which are worth noting. As is commonly observed for spin crossover compounds, all the Fe-N bond distances decrease by ~0.2 Å as the structure goes from HS to LS. In this case the range of Fe-N bond lengths in **A** decreases from 2.127(3) - 2.218(3) Å at 375 K to 1.955(2) - 2.014(2) Å at 30 K with the change in each unique Fe-N bond length through the spin crossover temperature range (Figure 5) following the trend observed in the magnetic data.[35, 36] The thermal HS to LS crossover for **A** is accompanied by a decrease in the distortion parameter (Σ) and volume of the Fe octahedron (V_p), see Table 3 and ESI Table S3. There is no significant change in unit cell parameters, Σ and V_p between crystal structures of **A** collected at 225 K (~ $T_{1/2}$) during cooling (↓) and warming (↑) cycles through the spin crossover (ramp rate 120 K/hr) (ESI Table S2). This is consistent with the magnetic data,[36] and indicates that thermal hysteresis is not observed for **A**. A gradual reduction in the diffraction quality occurs as a result of the spin crossover and after prolonged irradiation fracturing of the crystal was visible to the eye. The spin crossover in **2A** caused no apparent reduction in crystallinity[29] so it is unclear why the structural integrity of the crystal lattice of **A**, which is isostructural to **2A**, is more sensitive to the spin crossover.

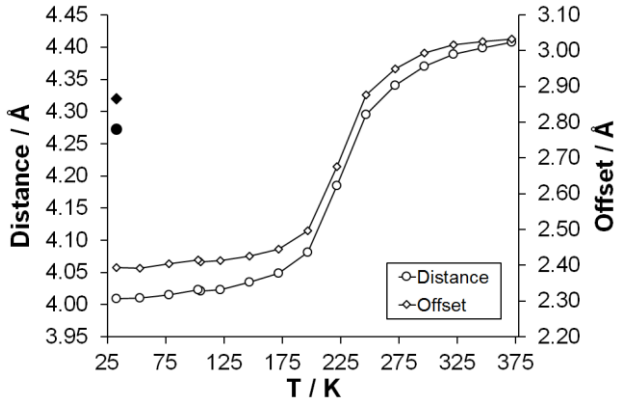

Figure 6 - Change in centroid-centroid separation between (N2, C2-C6) and (N2#4, C2#4-C6#4, #4 = 2-*x*, 1-*y*, 1-*z*) pyridyl rings: (○) distances and (◊) offsets as a function of temperature; (●) distance and (♦) offset for the LIESST HS* structure. Note: The values for these interaction parameters lie beyond those typically associated with a π-π interaction. Error bars are included but obscured by the data point markers.

In both **A** and the isostructural sulfur complex, $[Fe(abpt)_2(NCS)_2]$ polymorph **A** (**2A**), the HS to LS spin crossover results in a shortening of the intramolecular C2-H2···N4#1 (#1 = 1-*x*, 1-*y*, 1-*z*) interaction distance.[29] As indicated by the reduction in Σ, all the N-Fe-N bond angles get closer to 90° upon cooling through the HS to LS spin crossover. The N2-Fe1-N3 angle increases from 74.8(1)° at 375 K to 79.9(1)° at 30 K and there is a concomitant decrease in the N2-Fe-N3#1 (#1 = 1-*x*, 1-*y*, 1-*z*) angle from 105.2(1)° at 375 K to 100.1(1)° at 30 K. Similar changes in the N-Fe-N bond angles with temperature are observed for **2A**.[29] The π-π contacts between symmetry related pyridyl rings (N2, C2-C6) and (N7#3, C9#3-C13#3, #3 = 1-*x*, 2-*y*, 1-*z*), the intramolecular N6-H6B···N7 hydrogen bond and intermolecular N6-H6A···Se1#2 (#2 = 1/2+*x*, 3/2-*y*, 1/2+*z*) interaction all show either limited or no change across the investigated temperature range (ESI Table S4 and S5).

As a result of the spin crossover significant shifting of adjacent molecules is observed. This can be illustrated nicely by looking at the change in the centroid-centroid distance between two of the adpt ligands pyridyl rings (N2, C2-C6) and (N2#4, C2#4-C6#4, #4 = 2-*x*, 1-*y*, 1-*z*) in neighbouring molecules. Clearly, the separation and offset of these rings are beyond those typically associated with π-π interactions and hence no inference of a significant interaction is intended (Figure 6, Figure 7), however, it is worth noting that a similar change is also observed for **2A** as a result of the spin crossover.[29]

Table 3 - Fe-N bond lengths for all structures, along with the distortion parameter, Σ, and the volume of the Fe octahedron, V_p.

	30(2) K LIESST HS*	30(2) K	125(2) K	150(2) K	175(2) K	225(2) K	275(2) K	325(2) K	375(2) K
Fe1-N1 / Å	2.115(3)	1.955(2)	1.951(2)	1.950(2)	1.958(2)	2.032(3)	2.120(3)	2.137(4)	2.149(4)
Fe1-N2 / Å	2.185(3)	2.014(2)	2.014(2)	2.013(2)	2.021(2)	2.096(2)	2.193(2)	2.215(3)	2.218(3)
Fe1-N3 / Å	2.100(3)	1.956(2)	1.957(2)	1.955(2)	1.961(2)	2.027(2)	2.107(2)	2.124(3)	2.127(3)
Σ[a] / º	67.4(8)	49.5(6)	50.0(5)	49.8(6)	51.0(6)	59.0(6)	68.3(6)	69.4(8)	70.2(8)
V_p[b] / Å^3	12.524(11)	10.105(8)	10.087(6)	10.067(6)	10.174(7)	11.234(8)	12.629(9)	12.939(12)	13.029(12)

[a] Σ, the angle distortion parameter, is the sum of the absolute value of the deviation of all 12 *cis* N-Fe-N angles from 90°. [b] V_p is the volume of the Fe octahedron calculated in Olex2.[47]

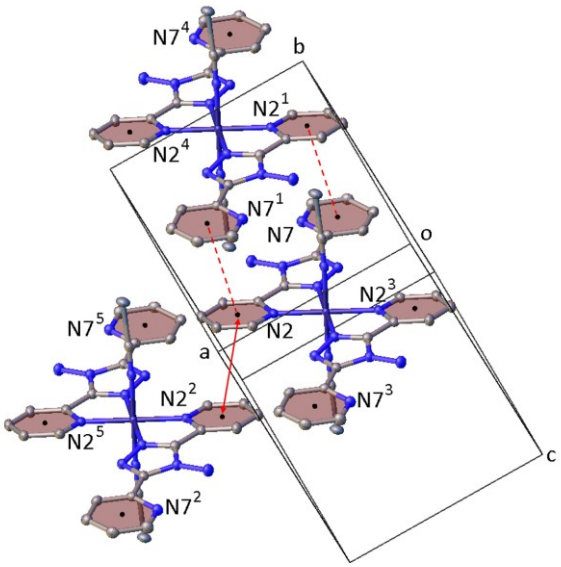

Figure 7 - Illustration of (red dashed lines) the π-π contact between (N2, C2-C6) and (N7[1], C9[1]-C13[1]) and (red solid arrow) the centroid-centroid separation distance between (N2, C2-C6) and (N7[2], C9[2]-C13[2]) that decreases as a function of temperature. Symmetry codes: [1] 1-*x*, 2-*y*, 1-*z*; [2] 2-*x*, 1-*y*, 1-*z*; [3] 1-*x*, 1-*y*, 1-*z*; [4] +*x*, 1+*y*, +*z*; [5] 1+*x*, +*y*, +*z*.

LIESST metastable HS* structure at 30 K

A critical LIESST temperature, T_{LIESST}, of ~32 K has been reported for **A** from magnetic measurements on a microcrystal sample.[36] The sulfur analogue, **2A**, which displays T_{LIESST} ~ 40 K, relaxes from the HS* state back to the LS state within ~4000 s[29, 36] at 30 K whereas **A** relaxes on a much quicker timescale. At 10 K, less than 20% of the HS* state of **A** exists beyond 500 - 1000 s and complete conversion back to the LS state is observed within <4000 s.[36] As the T_{LIESST} is only just above the minimum temperature of 30 K achievable on the in-house HeliX and given the rapid relaxation times in order to try and maintain a photostationary LIESST HS* structure throughout the data collection, the sample was subjected to continuous *in-situ* laser irradiation (670 nm, 5 mW CW laser). The structural changes observed in the resultant structure were consistent with those expected for a LS to HS* state spin crossover, i.e. the geometric parameters were similar to those seen in the HS structures collected around room temperature, indicating the successful formation of the LIESST metastable HS* state of **A**. Since the key structural features of the HS* structure are very similar to those of the 275 K HS structure (Table 3) only a few key points are highlighted here. The HS* structure maintains the same monoclinic space group, $P2_1/n$, found in the HS and LS structures, with an ~3% increase in the unit cell volume relative to the 30 K LS structure. As expected the Fe-N bond lengths in the 30 K HS* structure [2.100(3) - 2.185(3) Å] are almost 0.2 Å longer than those in the 30 K LS structure [1.955(2) - 2.014(2) Å]. In addition, the distortion parameter and Fe octahedron volume also increase as a result of the LS to HS* spin crossover: from Σ = 49.5(6)° and V_p = 10.105(8) Å^3 (LS, 30 K) to Σ = 67.4(8)° and V_p = 12.524(11) Å^3 (HS*, 30 K). It is worth noting that it is unknown whether the crystals used in this study retained a residual ground state, LS, fraction even during continuous irradiation at 30 K and the potential for any resulting bias in the HS* structural parameters was not investigated.[50]

Variable temperature UV-Vis transmission spectroscopy

Single crystals of **A** are an intense red colour in the HS state and gradually change to darker red upon cooling and, similar to **2A**,[29, 36] a residual HS fraction may remain in the predominantly LS state at low temperature. It is therefore challenging to collect good quality transmission spectra, particularly at low temperature, and assignment of the UV-Vis absorption bands to particular transitions is beyond the scope of this study. Figure 8 shows normalised UV-Vis transmission spectra obtained from a single crystal fragment of **A** at 290 K (HS state), 190 K and 110 K (LS state) collected as part of a kinetic series slow cooling through the spin crossover. At 290 K, where **A** is purely in the HS state, the spectrum shows one main band at ~524 nm and an absorbance edge ~580 nm. Below 190 K the spin crossover is virtually complete, **A** is essentially in the LS state and there is very little further spectral change. The one featureless band shown in the 190 K and 110 K spectra sits at a slightly longer wavelength than that observed at 290 K, resulting is movement of the absorption edge to longer wavelengths, ~610 nm and is consistent with the darker red colour of the crystal. Magnetic studies on **A** have shown a residual γ_{HS} at low temperature of 16% for a precipitated polycrystalline sample[35] and 0% for a sample consisting of single crystals.[36] The crystal preparation method used in this study differs from previous reports[35, 36] and it is unknown whether there is any residual HS contribution to the low temperature LS spectra. The crystal mount contracts during cooling and the crystal was repositioned in the beam several times during the experiment to maintain consistent illumination, therefore calculation of the percentage HS to LS conversion is not possible from the UV-Vis spectra.

Figure 9 shows that, in the wavelength region investigated, the largest change in absorbance with temperature occurs in the ~530 - 710 nm region with a maximum at 594 nm. It is difficult to distinguish any other small systematic changes with

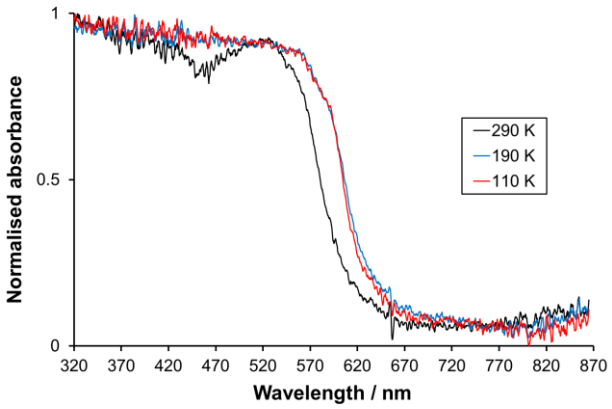

Figure 8 - Normalised UV-Vis absorbance spectra for $[Fe(abpt)_2(NCSe)_2]$ polymorph A at 290 K, 190 K and 110 K collected as part of a kinetic series cooling at 150 K/hr.

temperature from the noise, although there is a suggestion of a second transition centred around ~460 nm.

The transition shape and $T_{1/2}$ value reported from magnetic data for the thermal spin crossover in single crystals of **A**,[36] are closely mirrored in both the profile of the absorbance change with temperature at 594 nm (Figure 10) and the variable temperature crystallographic studies in this paper.

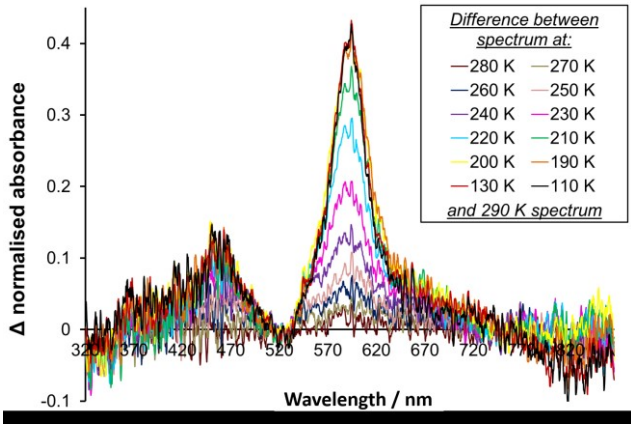

Figure 9 - Difference spectra for **A** calculated by ratioing the normalised absorbance spectrum at 290 K with spectra at various temperatures across the spin transition temperature range.

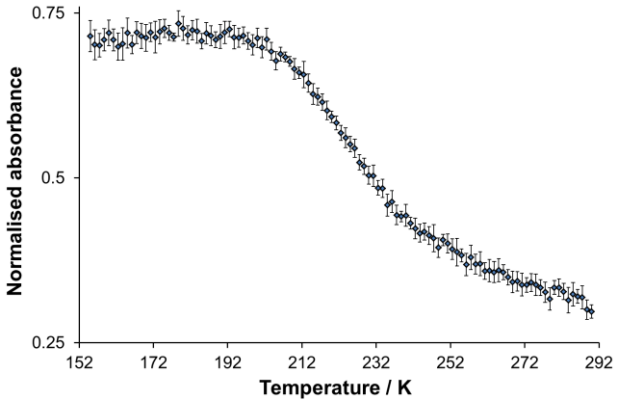

Figure 10 - Normalised absorbance spectrum for **A** showing the change in absorbance at 594 nm upon cooling at 150 K/hr through the thermal spin crossover temperature range. Note: Lower transmission intensity was observed between 154 - 132 K due to contraction of the crystal mount; at 132 K the mount was adjusted and spectra obtained between 132 - 83 K are consistent with those at 154 K, hence only data above 154 are presented.

Structural comparison of polymorphs A and B

Unlike **A**, polymorph **B** does not undergo a thermal spin crossover at ambient pressure.[40] The previously published structure of polymorph **B**[40] is used for the following discussions and comparison with polymorph **A** presented in this paper. Polymorph **B**, for which data were collected at 300 K, also crystallised in the monoclinic space group $P2_1/n$ with half a molecule in the asymmetric unit (Z' = 0.5, Z = 2). There are a number of similarities between the two polymorphs and in **B** the NCSe ligands are also approximately linear with an N-C-Se bond angle of ~179°, the NCSe ligands are also slightly bent with respect to the iron metal centre with an Fe-N-C angle of ~170°. In addition, the N-Fe-N angles between the NCSe and adpt ligands are in line with those seen for **A** ranging from ~87-93°. However, in **B** the adpt ligands are significantly distorted from planarity and there is an angle of ~36° between planes calculated through the two pyridyl ligands and ~7° and 31° between the 5 membered triazole ring and the two 6 membered rings respectively. This compares to values in **A** at 300(2) K of 9.4(2)° between the two pyridyl rings and 7.9(2)° and 7.5(2)° between the 5 membered and each of the pyridyl rings. This difference in configuration of the adpt rings may explain significant differences in the packing of the two polymorphs. In **A**, the three rings of the adpt ligands of adjacent molecules are aligned above each other with π-π interactions at each end between the pyridyl rings (at 300(2) K centroid to centroid distance 3.688(2), offset 1.339(6) Å) creating a 1-dimensional chain in approximately the *b*-axis direction. In **B**, each of the pyridyl rings on an adpt ligand forms π-π interactions (centroid to centroid distance ~3.73 Å, offset ~1.26 Å) with the pyridyl ring of adpt ligands that are on different molecules, creating a 2-dimensional network approximately parallel to the *ac* plane. Given the relatively gradual nature of the spin crossover in **A** it seems reasonable to suggest that there is limited communication between the molecules. The influence of intermolecular interactions and communication between the metal centres on the spin crossover behaviour of a compound is well documented. In this case it would appear reasonable to suggest that the lack of spin crossover in **B** is as a result of the 2-dimensional nature of the π-π interactions in **B** having affected communication between the metal centres as compared to **A** which forms a 1-dimensional chain as result of the pi-pi interactions involving the two pyridyl rings of both adpt ligands.

Conclusions

Structural and spectral changes associated with the spin crossover behaviour of $[Fe(abpt)_2(NCSe)_2]$ polymorph **A** have been successfully characterised. A clear shift is observed between the absorbance spectra obtained for the high and low spin complexes, monitoring the spectral changes in this region as a function of temperature shows a change consistent with the spin crossover observed in the previously published magnetic data. Likewise, the unit cell parameters change as a function of temperature with a profile that matches those observed in the magnetic data and supports the occurrence of spin crossover. The Fe-N bond lengths, distortion parameter (Σ) and volume of the Fe octahedron (V_p) all decrease as a result of the HS to LS spin crossover and follow the trends commonly associated with spin crossover complexes. It is interesting to note that for both **A** (NCSe) and **2A** (NCS),[29] the HS to LS spin crossover causes a shifting of adjacent molecules towards each other. This change was apparent in **A** through a change in distance between two of the adpt ligands pyridyl rings (N2, C2-

C6) and (N2#4, C2#4-C6#4, #4 = 2-*x*, 1-*y*, 1-*z*) in neighbouring molecules, although it should be noted that the separation distance between pyridyl rings remains beyond that associated with significant π-π interactions. A LIESST HS* structure for $[Fe(abpt)_2(NCSe)_2]$ polymorph **A** at 30 K is also reported and shown to have similar features to the HS structure at approximately room temperature. Comparing the structures of polymorphs **A** to **B** (which had been previously published and does not show a thermal spin transition at ambient pressure), shows clear differences in the relative orientations of the pyridyl rings on the same adpt ligand with twist angles of 9.4(2)° and ~36° respectively. The packing was found to be quite different for the two polymorphs with **A** having 1-dimensional chains created by π-π interactions between pairs of adpt ligands on adjacent molecules in which both pyridyl groups were involved while in **B** the π-π interactions formed a 2-dimensional network as a result of each pyridyl ring on an adpt ligand forming an interaction to the pyridyl ring on an adpt ligand in different molecules. Given the importance of intermolecular interactions on the spin crossover behaviour of compounds it seems reasonable to suggest that the nature of the interactions in **B** have affected the communication between metal centres and thus accounts for the lack of spin crossover for this polymorph.

Conflicts of interest

There are no conflicts to declare.

Acknowledgements

H. E. M. is grateful to Professor Jonathan W. Steed (Durham University) for useful discussions. She is also grateful to the EPSRC and Durham University for financial support.

References

1. L. Cambi and L. Szegö, *Berichte Der Deutschen Chemischen Gesellschaft*, 1931, **64 (10)**, 2591-2598.
2. A. Bousseksou, G. Molnar, L. Salmon and W. Nicolazzi, *Chem. Soc. Rev.*, 2011, **40**, 3313-3335.
3. M. A. Halcrow, *Chem. Soc. Rev.*, 2011, **40**, 4119-4142.
4. M. D. Manrique-Juarez, S. Rat, F. Mathieu, D. Saya, I. Seguy, T. Leichle, L. Nicu, L. Salmon, G. Molnar and A. Bousseksou, *Applied Physics Letters*, 2016, **109**.
5. P. Gütlich and H. A. Goodwin, eds., *Spin Crossover in Transition Metal Compounds I, II and III*, Springer-Verlag: Berlin, Heidelberg, New York, 2004.
6. M. A. Halcrow, ed., *Spin-Crossover Materials: Properties and Applications*, John Wiley & Sons, Ltd.: Chichester, UK, 2013.
7. O. V. Farberovich and V. L. Mazalova, *Journal of Magnetism and Magnetic Materials*, 2016, **405**, 169-173.
8. M. D. Manrique-Juarez, S. Rat, L. Salmon, G. Molnar, C. M. Quintero, L. Nicu, H. J. Shepherd and A. Bousseksou, *Coord. Chem. Rev.*, 2016, **308**, 395-408.
9. B. Doistau, L. Benda, B. Hasenknopf, V. Marvaud and G. Vives, *Magnetochemistry*, 2018, **4**.
10. P. Gütlich, A. B. Gaspar and Y. Garcia, *Beilstein J. Org. Chem.*, 2013, **9**, 342-391.
11. B. Fei, X. Q. Chen, Y. D. Cai, J. K. Fang, M. L. Tong, J. Tucek and X. Bao, *Inorganic Chemistry Frontiers*, 2018, **5**, 1671-1676.
12. P. Gütlich, V. Ksenofontov and A. B. Gaspar, *Coord. Chem. Rev.*, 2005, **249**, 1811-1829.
13. J. Laisney, H. J. Shepherd, L. Rechignat, G. Molnar, E. Riviere and M. L. Boillot, *Phys. Chem. Chem. Phys.*, 2018, **20**, 15951-15959.
14. A. Hauser, *Light-Induced Spin Crossover and the High-Spin→Low-Spin Relaxation.*, Springer-Verlag: Berlin, Heidelberg, New York, 2004.
15. A. Tsukiashi, M. Nakaya, F. Kobayashi, R. Ohtani, M. Nakamura, J. M. Harrowfield, Y. Kim and S. Hayami, *Inorg. Chem.*, 2018, **57**, 2834-2842.
16. H. S. Scott, R. W. Staniland and P. E. Kruger, *Coord. Chem. Rev.*, 2018, **362**, 24-43.
17. M. Nihei, T. Shiga, Y. Maeda and H. Oshio, *Coord. Chem. Rev.*, 2007, **251**, 2606-2621.
18. A. B. Gaspar, M. C. Muñoz, V. Niel and J. A. Real, *Inorg. Chem.*, 2001, **40**, 9-10.
19. P. Nielsen, H. Toftlund, A. D. Bond, J. F. Boas, J. R. Pilbrow, G. R. Hanson, C. Noble, M. J. Riley, S. M. Neville, B. Moubaraki and K. S. Murray, *Inorg. Chem.*, 2009, **48**, 7033-7047.
20. J. Tao, R.-J. Wei, R.-B. Huang and L.-S. Zheng, *Chem. Soc. Rev.*, 2012, **41**, 703-737.
21. I. Salitros, L. Pogany, M. Ruben, R. Boca and W. Linert, *Dalton Trans.*, 2014, **43**, 16584-16587.
22. H. Hang, B. Fei, X. Q. Chen, M. L. Tong, V. Ksenofontov, I. A. Gural'skiy and X. Bao, *Journal of Materials Chemistry C*, 2018, **6**, 3352-3361.
23. A. I. Vicente, L. P. Ferreira, M. D. Carvalho, V. H. N. Rodrigues, M. M. Dirtu, Y. Garcia, M. J. Calhorda and P. N. Martinho, *Dalton Trans.*, 2018, **47**, 7013-7019.
24. M. Griffin, S. Shakespeare, H. J. Shepherd, C. J. Harding, J.-F. Létard, C. Desplanches, A. E. Goeta, J. A. K. Howard, A. K. Powell, V. Mereacre, Y. Garcia, A. D. Naik, H. Mueller-Bunz and G. G. Morgan, *Angew. Chem., Int Ed.*, 2011, **50**, 896-900.
25. W. Liu, Y. Y. Peng, S. G. Wu, Y. C. Chen, M. N. Hoque, Z. P. Ni, X. M. Chen and M. L. Tong, *Angew. Chem., Int Ed.*, 2017, **56**, 14982-14986.
26. A. Schober, S. Demeshko and F. Meyer, *Zeitschrift Fur Anorganische Und Allgemeine Chemie*, 2018, **644**, 719-728.
27. L. Li, A. R. Craze, R. Akiyoshi, A. Tsukiashi, S. Hayami, O. Mustonen, M. M. Bhadbhade, S. Bhattacharyya, C. E. Marjo, Y. Wang, L. F. Lindoy, J. R. Aldrich-Wright and F. Li, *Dalton Trans.*, 2018, **47**, 2543-2548.
28. S. De, L. M. Chamoreau, H. El Said, Y. L. Li, A. Flambard, M. L. Boillot, S. Tewary, G. Rajaraman and R. Lescouezec, *Frontiers in Chemistry*, 2018, **6**.
29. H. E. Mason, W. Li, M. A. Carpenter, M. L. Hamilton, J. A. K. Howard and H. A. Sparkes, *New J Chem*, 2016, **40**, 2466-2478.
30. A. I. Rykov, J. Wang, T. Zhang and K. Nomura, *Hyperfine Interactions*, 2013, **218**, 139-143.
31. L. Pogany, B. Brachnakova, J. Moncol, J. Pavlik, I. Nemec, Z. Travnicek, M. Mazur, L. Bucinsky, L. Suchanek and I. Salitros, *Chem. -Eur. J.*, 2018, **24**, 5191-5203.

32. D. R. Zhu, Y. Xu, Z. Yu, Z. J. Guo, H. Sang, T. Liu and X. Z. You, *Chem. Mat.*, 2002, **14**, 838-843.
33. R. W. Hogue, R. G. Miller, N. G. White, H. L. C. Feltham, G. N. L. Jameson and S. Brooker, *Chem. Commun.*, 2014, **50**, 1435-1437.
34. J. A. Kitchen, G. N. L. Jameson, J. L. Tallon and S. Brooker, *Chem. Commun.*, 2010, **46**, 3200-3202.
35. N. Moliner, M. C. Muñoz, P. J. van Koningsbruggen and J. A. Real, *Inorg. Chim. Acta*, 1998, **274**, 1-6.
36. N. Moliner, M. C. Muñoz, S. Létard, J. F. Létard, X. Solans, R. Burriel, M. Castro, O. Kahn and J. A. Real, *Inorg. Chim. Acta*, 1999, **291**, 279-288.
37. C.-H. Shih, C.-F. Sheu, K. Kato, K. Sugimoto, J. Kim, Y. Wang and M. Takata, *Dalton Trans.*, 2010, **39**, 9794-9800.
38. C.-F. Sheu, C.-H. Shih, K. Sugimoto, B.-M. Cheng, M. Takata and Y. Wang, *Chem. Commun.*, 2012, **48**, 5715-5717.
39. C.-F. Sheu, S.-M. Chen, S.-C. Wang, G.-H. Lee, Y.-H. Liu and Y. Wang, *Chem. Commun.*, 2009, 7512-7514.
40. A. B. Gaspar, M. C. Muñoz, N. Moliner, V. Ksenofontov, G. Levchenko, P. Gütlich and J. A. Real, *Monatsh. Chem.*, 2003, **134**, 285-294.
41. A. E. Goeta, L. K. Thompson, C. L. Sheppard, S. S. Tandon, C. W. Lehmann, J. Cosier, C. Webster and J. A. K. Howard, *Acta Crystallogr., Sect. C: Cryst. Struct. Commun.*, 1999, **55**, 1243-1246.
42. Bruker, *SMART-NT, Data Collection Software, Version 5.63, Bruker Analytical X-ray Instruments Inc., Madison, WI, USA*, 2000.
43. Bruker, *SAINT-NT, Data Reduction Software Ver. 6.14, Bruker Analytical X-ray Instruments Inc., Madison, WI, USA*, 2000.
44. Bruker, *SAINT+ Integration Engine, Data Reduction Software, Bruker Analytical X-ray Instruments Inc., Madison, WI, USA*, 2007.
45. Bruker, *SADABS, Bruker AXS area detector scaling and absorption correction, Bruker Analytical X-ray Instruments Inc., Madison, Wisconsin, USA*, 2001.
46. G. M. Sheldrick, *Acta Crystallogr., Sect. A: Found. Crystallogr.*, 2008, **64**, 112-122.
47. O. V. Dolomanov, L. J. Bourhis, R. J. Gildea, J. A. K. Howard and H. Puschmann, *J. Appl. Crystallogr.*, 2009, **42**, 339-341.
48. M. R. Probert, *SMARTreduce, Durham University, UK*, 2009.
49. *MathWorks, MATLAB and Statistics Toolbox Release 2013a. 8.1.0.604 ed.; The MathWorks, Inc.: Natick, Massachusetts, United States*, 2013, **Vol. 2013a**.
50. V. Legrand, S. Pillet, H.-P. Weber, M. Souhassou, J.-F. Létard, P. Guionneau and C. Lecomte, *J. Appl. Crystallogr.*, 2007, **40**, 1076-1088.